Chapter 3
Fire-Resistant Steel

Abstract This chapter is concerned with the design and characterisation of fire-resistant steels for building construction. Issues raised include effects of alloy additions, controlling the grain size, properties of substitutional elements, and processing, centred on the property requirements for fire-resistant steels. The new fire-resistant steels are microalloyed with molybdenum and niobium, or tungsten, titanium and boron, as the alloying additions for elevated temperature strength. The steels have satisfactory high temperature strength, owing partly to their relatively large grain sizes compared with conventional steels. The nature of equilibrium precipitation is calculated using thermodynamics. The high temperature strengthening mechanisms could be attributed to secondary formation of fine distribution of MC and Laves phase precipitates, molybdenum clusters, and molybdenum and niobium in solid solution. The atomic-scale microstructure of structural steels designed to have fire-resistant microstructures is characterised using atom probe field ion microscopy (APFIM). There is strong precipitation at approximately 650 °C. These probably coherent precipitates have the effect of producing a stable dispersion.

3.1 Design Against Fire

Steel design is an immensely complex area. A process of iteration is required to refine the properties until they are optimal. A structural steel has well-known requirements as far as mechanical properties are concerned. Fire-resistant steels have the additional constraint of requiring an adequate level of strength at elevated temperatures reached in a fire.

Fire protection is needed because conventional structural steel cannot withstand the temperatures experienced in real fires. Many tests were carried out on various large-scale constructions at Cardington Laboratory in England as part of a European collaboration and co-ordinated by the Building Research Establishment (BRE) and the formerly British Steel. Most of the steelwork involved was unprotected and the temperatures of the steel members were recorded. Maximum steel temperatures between 691 and 1060 °C were recorded. If these temperatures are reached, then the limiting stress of the steel falls below the working stress and failure ensues. Thus, it is necessary to protect steelwork and ensure that such temperatures are not reached within the specified fire resistance period.

W. Sha, *Steels*, DOI: 10.1007/978-1-4471-4872-2_3,

A structural member must be able to perform its function during the designated fire resistance time. The specified fire resistance period for a building depends on its size, location and use, with the required period being given in multiples of 30 min, e.g. 30, 60, 90 min, etc. Approximately 7 % of all UK multi-storey steelwork requires 30 min fire resistance. 60 % requires 60 min fire resistance, 10 % requires 90 min fire resistance and 15 % requires 120 min fire resistance. The fire resistance of a member is assessed from the results of fire tests, based on the response of an individual member to the standard fire curve, following the prescribed temperature path. This, along with natural fire curves, depends on fire loads, measured in kilograms of wood and the amount of ventilation. The standard fire curve is different in nature to natural fires, but remains a useful means of comparing the fire resistance of structural members.

Given the impressive performance of the fire-resistant steels manufactured by Nippon Steel, it would seem sensible to use their compositions as a base from which to improve the properties further. This may be achieved by using additions of alloying elements and manipulating the processing variables. The compositions of these steels are given in Table 3.1.

The design can be approached from two different angles, i.e. to design 'intelligent' steel, which would react to a fire by precipitation, and 'solution' steel, which would simply resist the effects of a fire. The composition of steel can improve strength at high temperature, by precipitation hardening and solid solution strengthening. Each of these properties is, by their very nature, suited to the task of creating intelligent steel and solution steel, respectively. Solid solution strengthening provides a constant source of strength, although static, and thus, is suitable for solution steel. Precipitation is a dynamic, reactive process and is thus more suitable for intelligent steel. For carbide precipitates such as MC and M_2C and carbonitrides such as (V,Ti,Nb)(C,N), the source of strength becomes ineffective above approximately 650 °C, due to their dissolving and coarsening. It makes sense to give both the steels a small measure of each property, i.e. for one steel to be mostly solid solution strengthened with some precipitation and the other steel to be mostly precipitation-based with some solid solution strengthening. This approach would also lend itself to the reuse of steel after a fire. A certain amount of precipitation in the matrix would prevent grain growth both in ferrite and in austenite during a fire and hence loss of strength after a fire. This effect has already manifested itself in the Nippon fire-resistant steels.

3.2 Steel Design Considerations

3.2.1 Controlling the Grain Size

There is a definite need for a certain amount of precipitation in the steel in order to control the grain size during exposure to high temperatures and during the rolling procedure. However, if the objective is to study the viability of a solid solution

Table 3.1 Chemical composition of manufactured fire-resistant steels and conventional S275 structural steel (wt%)

Steel	C	Si	Mn	Mo	Nb	N	Other elements	Yield strength (MPa)	Tensile strength (MPa)	Elongation (%)
S275	0.1	0.35	0.9	–	–	0.001	–	280	318	19.5
Nippon Nb-Mo steel	0.11	0.24	1.14	0.52	0.03	0.004	–	350	552	20
Nippon Mo steel	0.1	0.1	0.64	0.51	–	0.003	–	380	507	21
Nippon Mo steel (2)	0.11	1.13	0.23	0.56	–	–		448	562	24
P8123 (Intelligent Steel)	0.08	0.38	1.32	0.54	0.26	0.001	–	594	723	13.5
P8124 (Solution Steel)	0.02	0.36	0.87	0.16	0.63	0.001	–	411	538	15.5
P8240 (low-alloying Solution Steel)	0.014	0.28	0.28	0.21	0.58	–	–	214	389	29
P8241	0.004	0.19	0.22	–	–	–	0.5W, 0.04Ti, 0.013Al, 0.001B	200	346	25

type of steel, the volume fraction of precipitation should be kept to a minimum. Another condition of the chosen carbide type must be that precipitation must occur at a high enough temperature to refine the grain size, i.e. at around 1,200 °C, implying carbide of the MX type. As only the most stable carbides precipitate at such high temperatures and form MC type, the choice of carbide forming elements is limited to titanium, zirconium and niobium. These elements result in the formation of MC-type carbides that not surprisingly are among the most stable carbides available, owing to their extremely high affinity for carbon. It is also important that the precipitation does not increase the yield strength of the steel too dramatically, if the objective is to concentrate on solid solution strengthening. Therefore, it is important that the amount of precipitation that occurs during and after the $\gamma \rightarrow \alpha$ transformation is strictly limited or preferably eliminated. Ti and Nb precipitate almost exclusively in the γ phase owing to their very low solubility.

An arbitrary level of carbon of 0.01 wt% would require a level of 0.04 wt% titanium, or 0.08 wt% niobium, to obtain stoichiometric TiC, or NbC, carbide. (All compositions in this chapter are given in wt%, unless otherwise indicated.) For Fe-0.01C-0.04Ti and Fe-0.01C-0.08Nb steels, thermodynamic calculations predict that TiC and NbC precipitates have solubility temperatures of 957 and 1072 °C, respectively. The addition of 0.5 % tungsten changed these values slightly to 956 and 1012 °C, respectively. A 0.01C-0.04Ti steel would have all of the carbon in TiC and leave tungsten in solid solution. For totally ferritic steel with only a small volume fraction of precipitation, a carbon level of 0.01 % and a titanium level of 0.04 % should suffice.

3.2.2 Properties of Substitutional Elements

In Table 3.2 are the atomic sizes of various substitutional elements that have a suitable range of solid solution in iron along with their shear modulus and the calculated diffusion rate at 850 °C. Unfortunately, there is no available information concerning calculation of the actual strain energy created by the modulus interaction. However, it can be observed that the shear modulus of tungsten differs from that of iron by the greatest amount, creating the greatest modulus interaction. After tungsten, the elements decrease in the order of niobium, molybdenum, titanium, vanadium. A high modulus interaction is desirable. A solute atom can interact with screw dislocations only in this way.

There is a huge variation in the range of diffusion rates. Tungsten has the ability to retard the self-diffusion of iron in iron-tungsten alloys. This was observed in iron alloyed with tungsten up to 0.33 at. %, where the self-diffusion coefficient of iron was drastically reduced. This effect was also observed in the iron-molybdenum system, although to a much lesser degree.

The total available strain energy is limited by the solubility of each solute, i.e. the limit of solubility where the Laves phase will form. Therefore, calculations were carried out to assess the solubility limit of each element. It was assumed that

Table 3.2 Various physical parameters of relevant elements being considered for design

Element	Fe	Mn	Mo	Nb	W	Ti	Cr	V	Co	Ni
Atomic radius R_x (Å)	1.24	1.3	1.36	1.42	1.36	1.45	1.25	1.31	1.25	1.15
Ratio R_x/R_{Fe}	1	1.05	1.10	1.15	1.10	1.17	1.01	1.06	1.01	0.93
Electronegativity	1.83	1.55	2.16	1.60	–	1.54	1.66	1.63	1.88	1.91
Shear modulus G_x (GPa)	82	80	126	38	161	46	115	47	82	76
$(G_x - G_{Fe})/G_{Fe}$ (%)	0	−3	54	−54	97	−44	41	−43	0	−7
Diffusion D in Fe at 850 °C ($\times 10^{-12}$ cm^2s^{-1})	7.9	21	21	96	9	1791	3.4	22	6.5	0.0002
Diffusion ratio D_x/D_{Fe} in γ at 950 °C	1	5	125	16	–	612	1.3	6	69	4
Diffusion ratio D_x/D_{Fe} in α at 700 °C	1	7	1.7	10	1.1	10	0.2	0.05	2.3	9×10^{-6}

the Laves phase will not form below 600 °C owing to under cooling and the very slow diffusion of substitutional elements. The weight percentage of each element was then obtained for this Laves phase solubility limit at 600 °C. The results were 1.8, 0.7, 0.8 and 17 wt% for molybdenum, tungsten, titanium and vanadium, respectively. Laves phase can tie up some of the niobium.

There are many factors to be weighed against each other in the choice of a major substitutional element for the fire-resistant steel. However, it is possible to eliminate unsuitable elements. Vanadium can be eliminated owing to its small shear modulus interaction. Niobium is unsuitable owing to its very fast rate of diffusion. Of the remaining elements, tungsten has a very large modulus interaction, titanium and molybdenum having considerably smaller values. All have Laves phase solubility limits above 0.5 %. However, it must be taken into account that tungsten has a slow diffusion rate in ferrite. This would hinder dislocation climb, as it is a diffusion-controlled event. Tungsten would also interact strongly with screw dislocations owing to its modulus interaction, whereas titanium has a weak modulus interaction. On this basis, tungsten can be the major substitutional element. Given that the Laves phase forms at 0.7 % at 600 °C, a level of 0.5 % should be appropriate for tungsten.

3.2.3 Processing, Steel Composition and Manufacturing

Consideration needs to be given to the effects of alloying elements and processing parameters. Tungsten is a ferrite stabiliser of approximately equal strength to niobium. Therefore, for a tungsten content of 0.5 %, it is certain that air cooled steel shall be entirely ferritic. Figure 3.1 is the phase diagram for

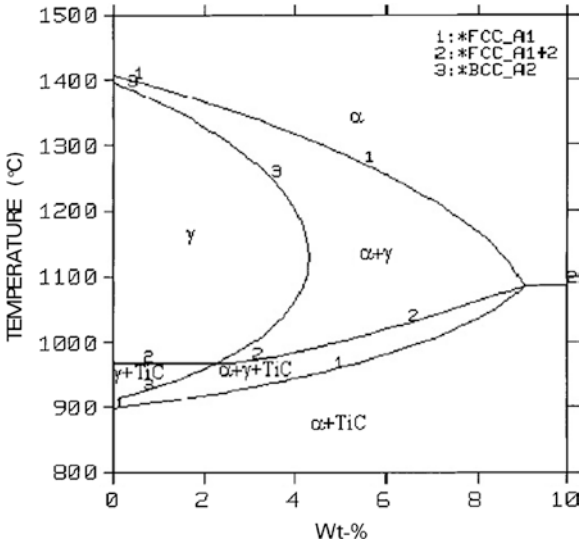

Fig. 3.1 Phase diagram for 0.01C-0.04Ti-0.1Si-0.2Mn (wt%) steel with varying temperature and W content. (From Sha et al. (2002), www.maney.co.uk/journals/mst and www.ingentaconnect.com/content/maney/mst.)

Table 3.3 Processing variables for experimental fire-resistant steels

Variable	Value
Cooling after rolling	Air cooled
Slab reheating temperature	1250 °C
Finish rolling temperature	1050 °C for P8123, P8124, P8240; 1000 °C for P8241
Thickness reduction factor	25 %
Number of passes	5
Initial plate thickness	75 mm
Final plate thickness	18 mm

0.01C-0.04Ti-0.1Si-0.2Mn steel alloyed with variable amount of W. The shape of the phase diagram is similar to those for stainless steels when significant levels of tungsten additions are employed. It can be seen that for a tungsten content of 0.5 %, the $\alpha + \gamma \rightarrow \gamma$ transformation temperature A_{e3} is ~920 °C and that the fcc TiC phase (line 2) should begin to precipitate at around 970 °C under equilibrium conditions. Owing to strain-induced precipitation after rolling, the actual precipitation temperature is likely to be considerably higher than that predicted.

The bulk compositions of the four experimental fire-resistant steels are given in Table 3.1, and the rolling parameters in Table 3.3.

3.3 Microstructure

3.3.1 Grain Structure

The microstructures of the steels are shown in Figs. 3.2 and 3.3 in the as-rolled condition and after heat treatment for 30 min at 650 °C (P8123 and P8124). These steels have similar grain structures.

The measured grain sizes in the as-rolled condition are 13 μm for the P8123 steel and 14 μm for the P8124 steel, compared with 6 μm for the Nippon fire-resistant steels. The grain size referred to here is the mean linear intercept, so the grains look larger in the photographs. The diameter of the grain is larger than the mean linear intercept by some 50 %. After the heat treatment, the grain sizes remain the same, showing no grain growth, which is as the case for the Nippon steels. These steels have polygonal ferrite microstructures, the P8123 steel also containing a proportion of acicular structure. There are large particles of the Laves phase, Fe_2Nb, in both P8123 and P8124 steels, particularly the P8124 (Fig. 3.4). This is expected for the P8124 steel, but is surprising in the case of the P8123 steel considering its lower niobium content.

The grain sizes are a little too large. A reduction in the finish rolling temperature from 1,050 to 1,000 °C results in a slightly smaller grain size.

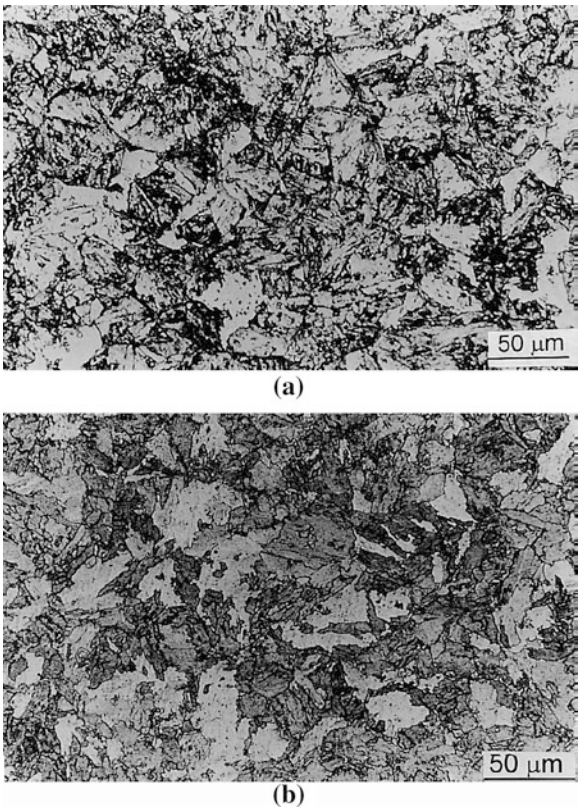

Fig. 3.2 Optical micrographs of P8123 steel. **a** As-rolled; **b** heat treated for 30 min at 650 °C. (From Sha et al. (2002), www.maney.co.uk/journals/mst and www.ingentaconnect.com/content/maney/mst.)

3.3.2 Ferrite–Austenite Transformation and Precipitation

The α–γ phase transformation (Fig. 3.5) temperatures are summarised in Table 3.4. The effect of the alloying elements is to push the ferrite to austenite transformation to higher temperature. This has benefits in strength retention at high temperatures, as the austenite phase is much softer than ferrite. Calculated using thermodynamics, A_{e1} is 679 and 877 °C for the P8123 and the P8124 steels, respectively. For P8240 and P8241, ferrite starts to transform to austenite (A_{e1}) at 946 and 934 °C, respectively.

Precipitates in the as-rolled P8123 steel are niobium rich compounds. The equilibrium ferrite matrix composition, from thermodynamic calculations, at

Table 3.4 α−γ transformation temperatures (°C)

Steel	A_{c1}	A_{c3}	A_{r1}	A_{r3}
P8124	927	939	853	863
P8240	944	952	901	913
P8241	968	989	909	915

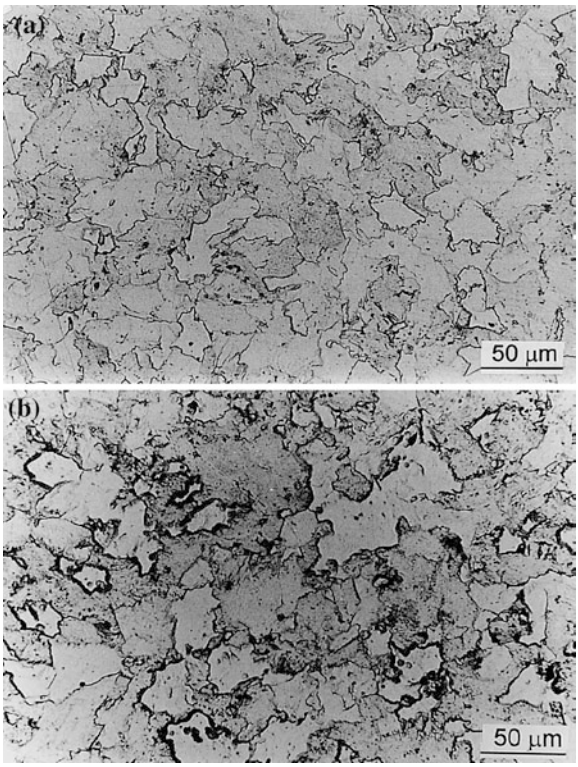

Fig. 3.3 Optical micrographs of P8124 steel. **a** As-rolled; **b** heat treated for 30 min at 650 °C. (From Sha et al. (2002), www.maney.co.uk/journals/mst and www.ingentaconnect.com/content/maney/mst.)

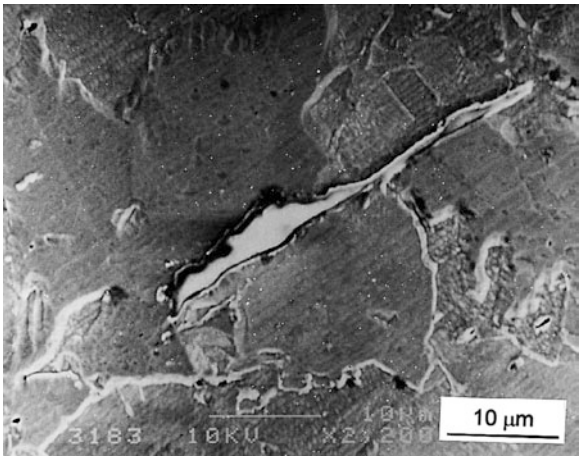

Fig. 3.4 Micrograph of large Fe_2Nb particle in P8124 steel in as-rolled condition (SEM). (From Sha et al. (2002), www.maney.co.uk/journals/mst and www.ingentaconnect.com/content/maney/mst.)

20 °C is Fe-0.39Si-0.72Mn. The calculated compositions of the precipitates at 20 and 650 °C are given in Table 3.5. Comparing the phase constitutions in addition to ferrite, at the two temperatures, cementite has disappeared at the higher

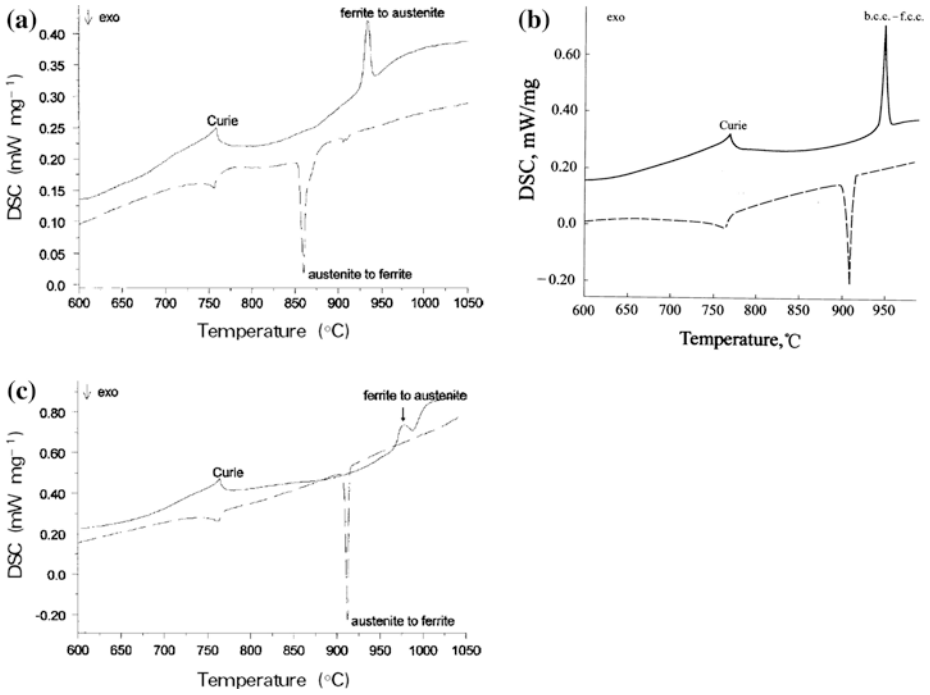

Fig. 3.5 Differential scanning calorimetry (DSC) curves: solid line is from heating and dashed line cooling. **a** P8124; **b** P8240; **c** P8241. ((**a**) and (**c**) from Sha et al. (2002), www.maney.co.uk/journals/mst and www.ingentaconnect.com/content/maney/mst.)

Table 3.5 Precipitate compositions (at.%) and mole fractions for P8123 and P8124 steels calculated

Steel	Temperature	Precipitate	C	Mn	Mo	Nb	Fe	Mole fraction of phase
P8123	20 °C[a]	Cementite	25	75.0	0.0	0.0	0.0	0.008
		M_2C	33.3	11.6	1.5	53.6	0.0	0.003
		M_6C	14.3	–	57.1	–	28.6	0.005
P8123	650 °C	NbC	49.9	0.2	7.6	42.3	0.0	0.004
		MoC	50	–	50	–	–	0.003
P8124	20 °C[a]	Nb_2C	33.3	0.0	0.0	66.7	0.0	0.003
		$Fe_2(Nb,Mo)$	–	–	10.9	22.5	66.7	0.009

[a]The equilibrium cannot be even approached at this low temperature after air cooling

temperature, as the MC-type carbides are the more stable phases. This correlates with the disappearance of cementite from the micrograph in Fig. 3.2b.

The equilibrium ferrite matrix composition at 20 °C calculated is Fe-0.37Si-0.88Mn. The composition of the Laves phase is given in Table 3.5. Silicon has an

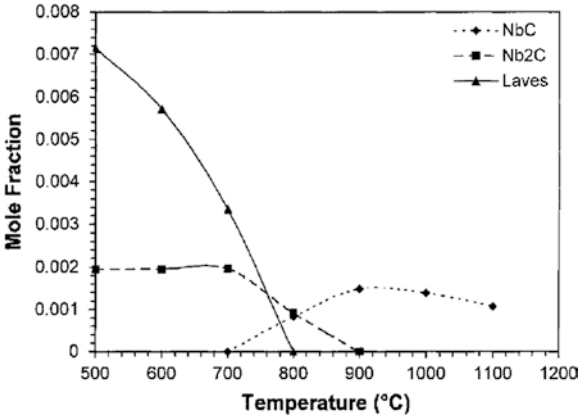

Fig. 3.6 Mole fractions of precipitate phases in P8240 steel as functions of temperature, as calculated thermodynamically. (From Sha et al. (2002), www.maney.co.uk/journals/mst and www.ingentaconnect.com/content/maney/mst.)

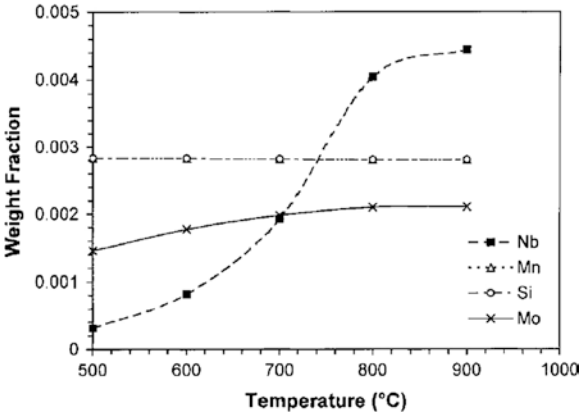

Fig. 3.7 Composition of ferrite phase in P8240 as function of temperature. Data points for Mn and Si overlap in the diagram. (From Sha et al. (2002), www.maney.co.uk/journals/mst and www.ingentaconnect.com/content/maney/mst.)

effect of lowering the solubility of niobium in iron and promotes the formation of the Laves phase. Silicon levels are around 15 % in Fe_2Nb precipitates for 1Si-2Nb steel. Silicon may decrease the lattice parameter of Fe_2Nb, reducing the required volume expansion of the matrix from 13.8 to 12.2 % and thus, facilitating nucleation. Silicon also results in a decrease in the niobium content of the Laves phase. These effects of silicon are not recognised in the thermodynamic database but are confirmed in experimental data (Sect. 3.3.4).

Equilibrium fractions of various phases as functions of temperature can be calculated thermodynamically, giving the variations of the mole fractions of precipitate phases (Fig. 3.6) and of the ferrite composition (Fig. 3.7) with increasing temperature. The Laves phase takes the form of $Fe_2(Nb,Mo)$, with the atomic fraction of Mo decreasing from 5 % at 500 °C to 2 % at 700 °C. At a temperature of 800 °C, two phases should co-exist, Nb_2C and NbC. Only NbC has been observed.

TiC with a slight deficiency in carbon at ~47 at.%, and Fe_2B phases exist in the equilibrium in P8241 steel up to 1,000 and 800 °C, respectively, but their

quantities are very minute, owing to the low carbon and boron contents in the steel. In addition, Fe_2W is also present in calculated equilibrium, up to 500 °C, although it is not expected to form at such low temperatures owing to kinetic reasons. The steel is thus almost entirely solid solution strengthened.

The steels are unlikely to exhibit equilibrium microstructures, given the heat treatment duration and the cooling rate. However, thermodynamic calculations show the possible phases and their maximum amounts, and show the partition and therefore to some degree the effectiveness of the alloying elements.

3.3.3 Nippon Fire-Resistant Steels

3.3.3.1 Matrix Compositions and Cementite

There are several notable features. There is very little carbon in solid solution in the matrix. Secondly, the majority of molybdenum is in solid solution, although somewhat surprisingly, the molybdenum level in solution is lower in the Nb–Mo steel than in the Mo steel. The difference, with respect to bulk composition, in measured molybdenum content is related to the consumption of this element in grain boundary segregation and molybdenum rich precipitates. These will be discussed in more detail later in Sect. 3.3.3.2. Lastly, the silicon level in the heat treated Nb–Mo steel is significantly higher than the nominal level. This suggests that there is a low solubility of silicon in the cementite, which would increase the matrix level. The manganese level in the matrix of the Nb–Mo steel increases to almost the nominal level, after heat treatment. It is possible that the local segregation, which dissipated after heat treatment, in the as-rolled steel caused the difference, with respect to bulk composition, in measured manganese content.

Cementite compositions measured using atom probe are shown in Table 3.6. Cementite is not a very fine and densely distributed phase, compared to precipitates.

3.3.3.2 Grain Boundary Segregation and Precipitation

Field ion micrographs of a grain boundary in each type of steel are shown in Fig. 3.8. There are considerable levels of segregation of all interstitial and substitutional elements at grain boundaries in both steels.

Grain boundary segregation is a non-equilibrium phenomenon, so place to place variations in the extent of segregation are well expected. There are particularly high segregation levels for C and Mo, whereas Mn and Si have levels that are

Table 3.6 Cementite compositions (at.%) of the Nippon steels as-rolled

Steel	C	Fe	Mn	Si	Mo	Nb
Nb–Mo	26.9 ± 1.4	71.9 ± 1.4	0.3 ± 0.2	0.4 ± 0.2	0.4 ± 0.2	0.1 ± 0.1
Mo	23.1 ± 1.6	75.4 ± 1.6	0.6 ± 0.3	0.1 ± 0.1	0.9 ± 0.4	–

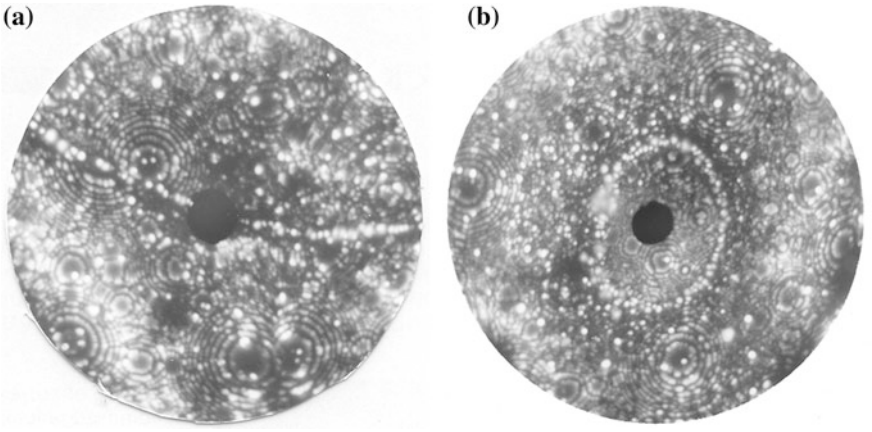

Fig. 3.8 Field ion micrographs of grain boundaries in two Nippon steels, both as-rolled. The distances across the images are 75 and 85 nm, respectively. **a** Nb–Mo steel; **b** Mo steel. (From Sha and Kelly (2004), www.maney.co.uk/journals/mst and www.ingentaconnect.com/content/maney/mst.)

more modest. The misfit energy of an atom provides the driving force for segregation. The misfit energy U of element is calculated from the following equation

$$U = 8\pi\mu r_0^3 \varepsilon^2 \tag{3.1}$$

where ε is the strain created by a foreign atom, μ is the shear modulus of the matrix and r_0 is the atomic radius of the matrix atom. The calculated values are shown in Table 3.7.

Carbon segregation at grain boundaries increases the yield strength by pinning grain boundary dislocations. This makes it more difficult for failure to propagate into the next grain. On the other hand, silicon has the opposite effect, acting in opposition to interstitial elements such as carbon and nitrogen by repelling them from the grain boundary, the so-called site competition effect. Low levels of silicon and high levels of carbon segregation would be beneficial to strength. In addition, the presence of slow diffusing elements such as molybdenum is beneficial to the hindrance of grain growth.

Increased rate of diffusion along grain boundaries is a well-known occurrence, boundary diffusion coefficients being approximately 105 times higher than matrix diffusion coefficients at a temperature of 0.6 T_m. Given this fact, it is almost certain that grain boundary precipitates will form as a secondary process to

Table 3.7 Misfit energy of elements

Steel	C	Mn	Si	Mo	Nb
U (kJ mol^{-1})	1420	26	149	182	280

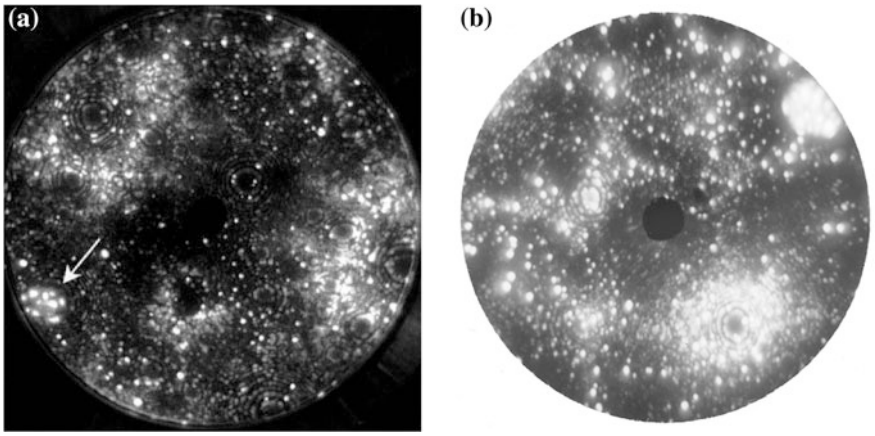

Fig. 3.9 Field ion micrographs of **a** an NbC precipitate in the Nb–Mo steel; **b** MoC precipitate in Mo steel (*top right* edge). (From Sha and Kelly (2004), www.maney.co.uk/journals/mst and www.ingentaconnect.com/content/maney/mst.)

segregation. There are similar segregation levels of molybdenum and carbon in a 0.2C–0.5Mo (wt%) steel.

Only MC-type precipitates are observed in the Nippon steels. Field ion micrographs of precipitates in steels are shown in Fig. 3.9. In addition to precipitates, clusters of molybdenum atoms are present in the steels before and, in larger numbers, after heat treatment.

3.3.4 Prototype Fire-Resistant Steels

The bulk compositions of the P8123 and P8124 steels are shown in Table 3.1. The compositions of the steels are also shown in Table 3.8 (at.%), along with the matrix (ferrite) compositions determined by thermodynamic calculations. At 20 °C, the equilibrium phases are ferrite (97.8 mol%), cementite (1.2 mol%), Fe_2Nb (0.5 mol%) and M_6C (Mo_4Fe_2C, 0.5 mol%). At 650 °C, the equilibrium changes to ferrite (99.3 mol%), NbC (0.4 mol%) and MoC (0.3 mol%). So, the

Table 3.8 Nominal compositions and calculated matrix compositions (20 °C) of prototype steels (at.%), with the balance being iron

Steel	Region	C	Si	Mn	Mo	Nb
P8123	Nominal	0.37	0.76	1.34	0.31	0.16
	Matrix	0.009	0.76	1.34	0.064	0.00
P8124	Nominal	0.09	0.72	0.88	0.09	0.38
	Matrix	0.00	0.72	0.88	0.08	0.05

Table 3.9 Precipitation compositions (at.%) determined by atom probe for P8123 and P8124 steels before and after heat treatmentheat treatment

Steel	Condition	Precipitate	C	Nb	Mo	Fe	Si	Mn
P8123	650 °C, 30 min	NbC	50 ± 3	35 ± 3	9 ± 2	6 ± 2	0	0
		MoC	46 ± 6	15 ± 4	33 ± 6	6 ± 3	0	0
P8124	As-rolled	Fe_2Nb	0	35.4 ± 1.5	1.5 ± 0.4	49.0 ± 1.6	13.0 ± 1.1	0.8 ± 0.3
	650 °C, 30 min	Fe_2Nb	0	33.8 ± 1.3	0.8 ± 0.3	50.6 ± 1.4	12.8 ± 0.9	1.5 ± 0.3

Fig. 3.10 Field ion micrograph of precipitate in P8123 steel after heat treatment. Distance across image is about 65 nm. (From Sha and Kelly (2004), www.maney.co.uk/journals/mst and www.ingentaconnect.com/content/maney/mst.)

carbon level in the as-rolled P8123 already bound up in cementite is released to form secondary carbides.

The average compositions of precipitates are shown in Table 3.9. After the heat treatment, NbC, MoC and Fe_2Nb are formed. A field ion micrograph of a typical precipitate in the heat treated P8123 steel is shown in Fig. 3.10. The total numbers of atoms analysed for different types of precipitates are reflected in the errors given in the table.

The apparent fine clusters in Fig. 3.10 are not all real clusters. Some are due to the strong field retention effects of elements such as molybdenum. However, it is expected that certain clusters do exist.

Due to the small size of carbide precipitates analysed by the atom probe, it is almost certain that there is some contribution from the matrix in the precipitate compositions, giving precipitate iron levels of about 6 %. In addition to the precipitates mentioned above, clusters of molybdenum atoms are also present in the P8123 steel before and after heat treatment. A typical cluster of molybdenum atoms is shown in Fig. 3.11a.

There are numerous extremely small precipitates present after heat treatment (Fig. 3.11b). Due to magnification effects of precipitates in field ion microscopy, it is notoriously difficult to estimate precipitate sizes from the micrographs. However, it is clear that there are many precipitates of around 1–2 nm in size.

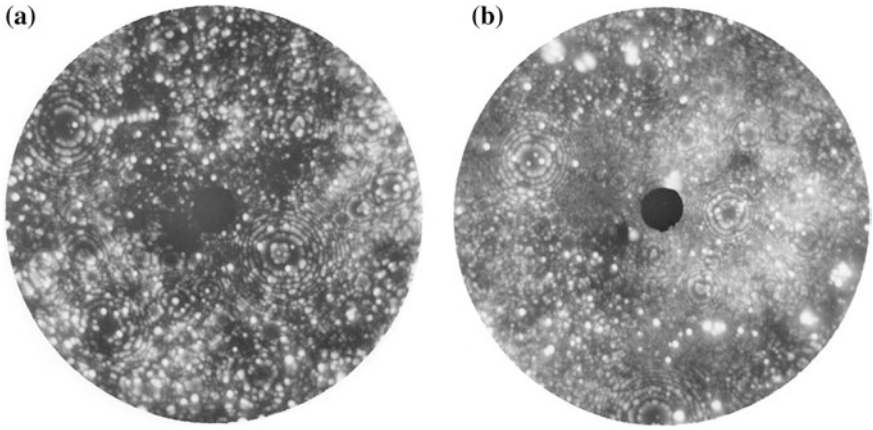

Fig. 3.11 **a** Field ion micrograph of molybdenum cluster in as-rolled P8123. Distance across image is about 75 nm. **b** Typically dense distribution of extremely fine MC precipitates after heat treatment. Distance across image is about 110 nm. (From Sha and Kelly (2004), www.maney.co.uk/journals/mst and www.ingentaconnect.com/content/maney/mst.)

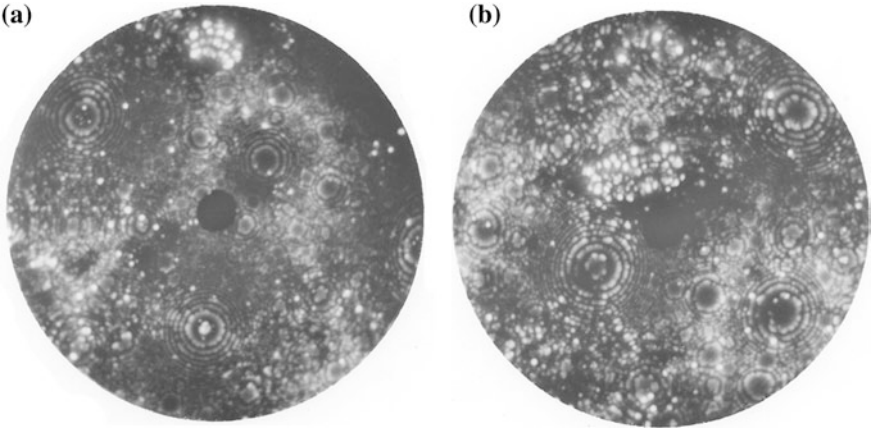

Fig. 3.12 **a** Field ion micrograph of Fe_2Nb precipitate in as-rolled P8124 steel. Distance across image is about 95 nm. **b** Field ion micrograph of Fe_2Nb precipitate in heat treated steel. Distance across image is about 65 nm. (From Sha and Kelly (2004), www.maney.co.uk/journals/mst and www.ingentaconnect.com/content/maney/mst.)

In the P8124 steel, only the ε-Laves phase, Fe_2Nb, is found, both in the as-rolled condition and after heat treatment at 650 °C for 30 min. The composition of these Fe_2Nb precipitates is included in Table 3.9. Field ion micrographs of typical Laves phase precipitates in the as-rolled and heat treated conditions are shown in Fig. 3.12. In addition, clusters of molybdenum atoms are present, although only in the heat treated condition.

The composition of the Laves phase by thermodynamic calculations (Sect. 3.3.2) is essentially stoichiometrically based on Fe_2Nb. For the P8124 steel, the calculated Laves phase composition is substantially different from the experimental composition. Experimental results show that the Laves phase has considerable levels of silicon and small amounts of manganese and molybdenum, none of which are present in the calculated Laves phase. The niobium content is also higher than that obtained by thermodynamic calculations.

3.4 Mechanical Properties

3.4.1 Strength

Yield strength (0.2 % proof strength) and tensile strength of the steels versus temperature are shown in Figs. 3.13 and 3.14, along with the values for the S275 steel for comparison. The steels were all in as-rolled state, with no heat treatments. The yield strength ratio of 60 % is a useful basis for comparison between the steels. Steels P8123 and P8124 reach 60 % strength at temperatures of 725 and 730 °C, respectively. This is a considerable improvement over the values of 625 and 645 °C exhibited respectively by the Nippon Nb–Mo and Mo steels and the value of 510 °C for the S275 steel. The steels exhibit work hardening up to 700 °C but such ceases to be apparent at 800 °C.

The low-alloying version of the Solution Steel is similar to P8124 but with lower alloying concentrations (including carbon). There is large stored energy in the P8240 steel because of rolling.

There are probably combinations of reasons for the strength loss of P8123 and P8124 steels above 700 °C. Grain boundary sliding may come into effect in this temperature range, as well as increased diffusion rates, leading to faster

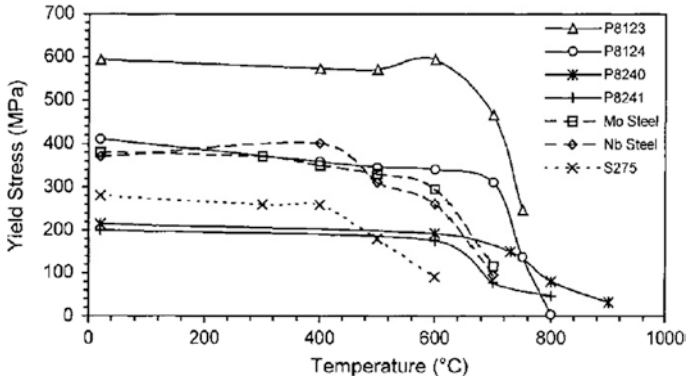

Fig. 3.13 Yield strength as function of temperature for fire-resistant steels and conventional constructional steel. (From Sha et al. (2002), www.maney.co.uk/journals/mst and www.ingentaconnect.com/content/maney/mst.)

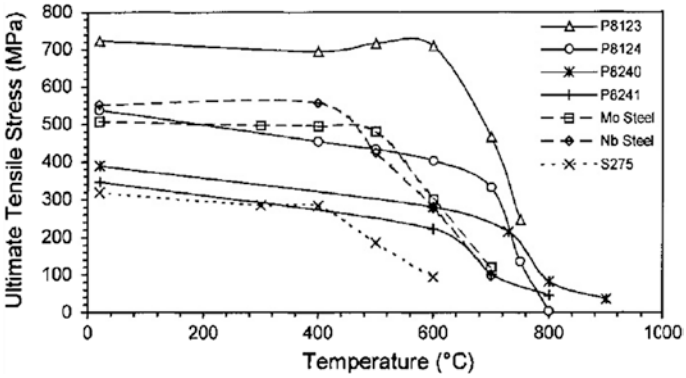

Fig. 3.14 Ultimate tensile strength as function of temperature for fire-resistant steels and conventional constructional steel for comparison. (From Sha et al. (2002), www.maney.co.uk/journals/mst and www.ingentaconnect.com/content/maney/mst.)

dislocation climb. For the P8123 steel, the loss of strength above 700 °C is also due in part to the progressive transformation of ferrite to austenite, which has been shown to start at around 704 °C from differential scanning calorimetry experiments. The transformation would have completed at 750 °C and precipitates coarsen rapidly and lose coherency at this temperature. There is a significant loss of strength associated with these phenomena.

For the P8124 steel, it is more difficult to assess the mechanism of strength loss. Thermodynamic calculations predicted that the Laves phase should go into complete solution at 756 °C. However, due to stabilisation of the Laves phase by silicon, an effect not considered in the database, this would not be expected to happen. TEM thin foil observation of tensile samples from 750 °C has confirmed that the Laves phase is present and its general morphology and distribution are unchanged. It is unlikely that grain boundary sliding contributes significantly to the loss of strength at 750 °C. There is an effect of inter-phase boundaries on grain boundary sliding. Grain boundary sliding, consisting of sliding and migration, is considerably reduced by the presence of inter-phase boundaries. Since the Laves phase grain boundary precipitates are present in the P8124 steel at 750 °C covering approximately 50 % of grain boundaries, the migration of these grain boundaries is highly unlikely. Therefore, the increased rate of diffusion and occurrence of vacancies and the resulting increase in dislocation climb are thought to be the main mechanisms of strength loss at 750 °C for the P8124 steel. Surprisingly, the Curie temperature, the change from the ferromagnetic to the paramagnetic conditions, may have a large impact on this mechanism.

Values of lattice friction stress (the resistance of the matrix to the motion of dislocations) for these steels at 600 °C are calculated to be 440 MPa for the P8123 steel and 192 MPa for the P8124 steel. These may be compared to 30, 72 and −92 MPa for the Nb–Mo, Mo and S275 steels respectively. The negative value of the S275 steel probably reflects the fact that grain boundary sliding occurs below this temperature or that the k_y value does not remain constant at these temperatures.

The high lattice friction stresses of the steels are due to the high volume fraction of precipitates, molybdenum clusters and the considerable amount of molybdenum and niobium in solid solution. In the P8123 steel, the particularly high friction stress is due to the distribution of extremely fine NbC precipitates. As for the Nippon steels, climb over these obstacles must occur for dislocations to move through the matrix. However, the process of climb is slower in the prototype steels.

3.4.2 Elongation and Fracture Surface

At room temperature, both P8123 and P8124 steels exhibit lower elongation than commercial steels. The loss of elongation for the steels at 600–700 °C is likely owing to carbide precipitation, which has been shown by DSC and thermodynamic calculations to occur at this temperature range. The rise in elongation after this temperature range suggests rapid overageing of these precipitates and/or enhanced climb at the higher temperatures. Low ductility at slow strain rates is a feature of age hardening alloys. The elongation of both P8123 and P8124 steels can be considered too low for a structural steel, being considerably lower than the commercial steels at almost every test temperature.

The poor elongation of the P8123 and P8124 steels was owing to the large amount of grain boundary precipitation of cementite (Sects. 3.3.2 and 3.3.4) and the Laves phase (Sect. 3.3). In addition, both the steels have high manganese contents, 0.87 % for the P8124 steel and 1.32 % for the P8123 steel. High Mn has a beneficial effect on the ductility of steels but this applies only to commercial steels that have a certain amount of sulphur. However, at high temperatures, manganese in solid solution decreases the ductility. Thus, this is a contributing factor to the poor high temperature elongation of the steels. It would therefore be advisable to reduce the manganese content in new steels, if they should be of high purity, containing virtually no sulphur. However, if the steel were to be produced commercially, manganese would certainly be required to control sulphide inclusions. A value of 0.2 % should be adequate.

The tensile fracture surfaces show that the poor ductility can be attributed to the presence of large Laves phase precipitates in the steels. Typical fracture surfaces for the P8123 and P8124 steels after conventional tensile testing at room temperature are formed by coalescence of dimples generally originated at large Laves phase particles, which are present on the fracture surfaces. The many small particles on the fracture surface for P8123 are carbides. The Laves phase particles are of the order of 5 μm in size.

3.4.3 Hardness and Creep

The hardness for the steels is shown in Fig. 3.15. The initial Vickers hardness values are 204 HV and 149 HV for the P8123 steel and P8124 steel respectively. The equivalent tensile strengths are 693 and 506 MPa, which are reasonably close to the experimental tensile values of 723 and 538 MPa for the P8123 and P8124 steel respectively. From 550–650 °C, P8123 steel shows a peak in hardness.

As this peak correlates well with microscopy observation of secondary precipitation and DSC precipitation peaks, it can be associated with MC precipitation and/or the formation of additional molybdenum clusters. The hardness values for the P8124 steel remain roughly constant over the whole temperature range, the small rise being within error limits but also perhaps indicative of a small amount of Laves phase or molybdenum cluster precipitation. This shows that the P8124 steel is indeed essentially non-ageing, in concordance with TEM and DSC observations.

A trend for all of the age-hardening steels is that the hardness value peaks during precipitation at around 650 °C, and then returns to a value that is slightly above the value before the precipitation peak, at say, 500 °C. The difference between the values after ageing at 500 and 700 °C could be explained by the presence of the greater number of precipitates which have precipitated between these temperatures. The Vickers hardness after heat-treatment at 650 °C for up to 3 h remains approximately constant.

Creep curves for P8240 and P8241 steels at 600 °C and 0.71 × σ_y, σ_y being room temperature yield stress, are similar to those from the other fire-resistant steels, namely P8123 and P8124, with the maximum creep strain reaching 0.18 % after three hours.

3.4.4 Connection Between Atom Probe Data and the Evolution of Mechanical Properties

Comprehensive mechanical properties of the steels at room and elevated temperatures, in the as-rolled state and after heat treatment, are given earlier. Of particular relevance to the atom probe data are the hardness measurements results of as-rolled steels and steels after ageing at 650 °C for 30 min, the conditions used for the steels in Sects. 3.3.3 and 3.3.4. The results for the two Nippon steels are given in Table 3.10.

The general observation is that the hardness of the two Nippon steels remains at about the same level as as-rolled hardness after heat treatment at 650 °C for 30 min. Note, however, that there is a significant decrease in hardness in the Nippon steels after treatment for the same length of time at all other temperatures (400–600 °C and 700 °C), and the hardness after the 650 °C treatment appears to

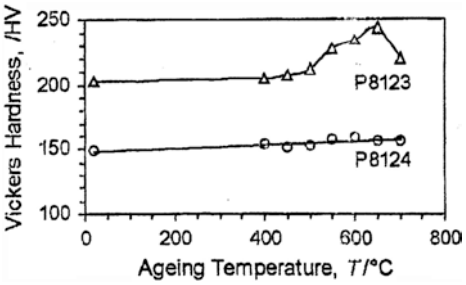

Fig. 3.15 Room temperature Vickers hardness values for the P8123 and P8124 steels after 30 min heat-treatment at various temperatures. (From Sha (2001).)

Table 3.10 Vickers hardness of Nippon fire-resistant steels before and after heat treatment

Steel	As-rolled	650 °C, 30 min
Nb–Mo	166	163
Mo	148	144

be a peak. The decrease in hardness is thought to be due to the recovery process of the deformed as-rolled steels. Therefore, ageing at 650 °C has caused significant hardening, although the hardness values appear to be similar to as-rolled hardness. Such hardening is caused by the additional precipitation and grain boundary segregation observed through atom probe field ion microscopy.

3.4.5 High Temperature Transient Tensile Properties

Section 3.4.6 is concerned with the properties of fire-resistant steels at high temperatures using transient tensile testing. Each country requires a similar minimum standard performance from structure during a fire over a specified period. For example when designing a structure for use by the public, in some specific situations that structure must be able to withstand a fire for two hours without major structural failure occurring. This means that structural steel members must usually be able to withstand air temperatures in excess of 1,000 °C over the required period.

The importance of metals as constructional materials is almost invariably related to their load bearing capacity in either tension or compression and their ability to withstand deformation without fracture. It is usual to assess these properties by tensile tests in which the modulus of elasticity, the yield or proof stress, the tensile strength and the percentage elongation are determined. A stress–strain curve is plotted using stress obtained by dividing the load by the original cross-sectional area of the specimen, and strain obtained as the extension divided by the original heated length. This curve is known as an engineering stress–strain curve and rises to a maximum stress level and then falls off with increasing strain until it terminates as the specimen breaks. The maximum stress level is known as the tensile strength of the specimen. Stress–strain curve shows a linear relationship from the origin up to the proportional limit point, also called elastic limit. This initial linear deformation is the elastic deformation of the material. This deformation is recovered once the load is removed from the specimen. This behaviour is called the elastic behaviour. The point at which the line begins to deviate from this linear characteristic is known as the elastic limit. After this point, any deformation that occurs will be plastic and so it is not recoverable.

In many structures, it is common for a loaded steel component to be in fire situation subjected to a change in temperature and it is important to know how the resulting deformation of the material will develop. For this reason, tensile tests under transient heating conditions have been devised. In such tests, the load on a steel specimen is maintained constant while its temperature is increased at a

given rate and the changes in gauge length are constantly recorded. Typical tensile curves are shown up to 2 % strain derived from transient tests at a heating rate of 10 °C per minute. The principal features comprise a small initial elastic extension, when the load is applied at room temperature, followed by a very gradual increase in length as the temperature is increased. For the purpose of fire engineering design, strength reduction factors can be derived from the transient tensile curves. These factors can be found by dividing the stresses at 2, 1.5 and 0.5 % strains by the yield strength of the material at room temperature (approximately 20 °C). Then strength reduction factor versus temperature curves can be plotted. The relationship between the elongation at fracture and temperature also can be derived from the transient tensile data.

3.4.6 High Temperature Transient Tensile Test

The building standards in the UK, Western Europe and North America are different from the standard in Japan, for fire resistance of steel structures. The Western codes are based on the strength reduction factors of steels, which are defined as the ratios of tensile stresses of steels at specific strain levels (e.g. 2 % for beams), at high temperatures, to room temperature yield stress. Normally, the tensile stresses at different strain levels are obtained easily with tensile tests, when a sample is held at a constant temperature while the stress–strain curve is obtained. However, in European building design codes, this test method is not acceptable for obtaining such stresses. Instead, a transient test must be used.

In the transient test, a tensile sample is held at a constant stress, or load, and the temperature is increased constantly, at a specified rate of 10 °C per minute. The strain is measured at short intervals. So, this is similar to a creep test, except that the temperature in a creep test is constant. The transient test will result in a strain-temperature curve. By conducting many such tests for a given material at many different stress levels, stress–strain curves for various temperatures can be built. British and European codes require the strength reduction factors to be obtained from stress–strain curves built in this way.

Essentially, the amounts of experimentation are similar for the two types of tests. The normal constant temperature tests (called steady-state test in Eurocodes) require many tests at various fixed temperatures with constantly increasing strain in each test, while the transient tests require many tests at various fixed stress levels with constantly increasing temperature in each test. However, the stress–strain curves built with transient tests usually give lower strength because in transient tests the samples are heated for a considerable length of time before the strain is taken, and this usually causes softening. For example, in a stress–strain curve at 620 °C, the steel will have been heated from 20 to 620 °C for an hour before the data are taken. However, the fire-resistant steels may well behave differently.

The author has been conducting research on fire-resistant steels since 1995. From the long contacts with British and European building industry, the largest

resistance of using the Nippon fire-resistant steels is because of a lack of knowledge and confidence. Although the Nippon steels are widely publicised, there are no transient test data, and therefore, there are no strength reduction factors data. The building designers cannot use Nippon steels when no appropriate materials strength data are available. The steel companies can dismiss Nippon steels for this simple reason. It is widely regarded in the West that the steels are only designed for Japanese market. The transient test results will demonstrate clearly the performance of Nippon steels, using test methods accepted in Western Europe.

3.5 Summary

Japanese Industrial Standards (JIS), "Rolled steels for welded structures" specifies chemical composition and mechanical properties at room temperature and does not specify mechanical properties at high temperature. Fire-resistant steel satisfies specification on JIS. The three fire-resistant steels, Nb-Mo steel, Mo steel and Mo steel (2) were made by Nippon Steel. The compositions of the steels are given in Table 3.1. The yield strength, tensile strength and elongation are also shown in Table 3.1, compared with the normal requirement for structural steel of yield strength between 300 and 400 MPa and an elongation of 20 %. A brief description of each alloying element used in the steels is shown in Table 3.11. Nb–Mo steel and Mo steel (2) are G3106 SM490A with tensile strength at room temperature higher and equal to 490 MPa because of the amount of manganese in their chemical composition. Mo steel is SM400A with tensile strength at room temperature higher and equal to 400 MPa. Structural steel should satisfy the weldability, and weld test like maximum hardness test in welded heat-affected zone (HAZ). The hardness of the heat-affected zone is lower for the fire-resistant steel than the conventional steel.

Given that carbon-based steels are characterised by ferrite to austenite transformation temperatures of 700–750 °C, and the relative instability of carbide precipitates above 650 °C, their use at high temperature is questionable. The greater resistance to ageing of the intermetallic Laves phase, Fe_2Nb, indicates that the use of intermetallic precipitates may be of great potential benefit for fire-resistant steels.

The better high temperature tensile strength and creep properties of the Nippon steels than conventional structural steels are due to the very fine distribution of MC precipitates, Mo clusters and molybdenum in solid solution. Grain boundary segregation also plays a role in improvement of high temperature mechanical properties. In addition, there is a strong secondary wave of precipitation at approximately 650 °C. These, probably coherent, precipitates have the effect of producing a very fine and stable dispersion.

For the prototype P8123 steel, 0.08C-0.38Si-1.32Mn-0.54Mo-0.26Nb, the high temperature strength is due to the distribution and secondary precipitation of ultra fine MC precipitates, as well as the molybdenum and niobium in solid solution. The mixed composition of these precipitates has the effect of producing a very fine dispersion of stable, coherent precipitates, which coarsen very slowly. For the

Table 3.11 Brief description of each alloying element used in the fire-resistant steels

Element	Description
C, carbon	An essential ingredient in steel. Higher carbon content increases the yield point and hardness and reduces ductility and weldability
Si, silicon	Higher silicon content increases the strength of the steel at high temperatures by raising the ferrite–austenite transition temperature
Mn, manganese	Manganese is similar in many ways to iron and is widely used in steel as deoxidant. Manganese can contribute to temperature embrittlement. It lowers the ferrite–austenite transition temperature and can therefore be used to stabilise silicon content in steel
Mo, molybdenum	The principal use of molybdenum worldwide is in alloy steel. It can help to reduce temper brittleness in steel. Molybdenum raises the high temperature strength and creep resistance of steel, but reduces the yield strength at room temperature. It does this by reducing the austenite-pearlite transformation temperature
Nb, niobium	Niobium improves the steel strength at room temperature and at high temperature without affecting weldability. It also improves creep strength

P8124 steel, 0.02C-0.36Si-0.87Mn-0.16Mo-0.63Nb, the high strength is due to precipitation of the Laves phase, which is stable and resists coarsening. The loss of strength at high temperatures is proposed to stem mainly from dislocation climb, and, in the case of the P8123 steel, the ferrite to austenite phase transformation, which reduces the strength dramatically.

The experimental steels developed, with nearly completely ferritic microstructures, have demonstrated high elevated temperature strength compared to the Nippon steels. The conclusion to be drawn from this is that good high temperature strength is not dependent on the presence of acicular transformation products such as acicular ferrite or bainite. The Nippon steels have such products that have been claimed to be responsible for good high temperature strength. The P8123 experimental steel performed extremely well, but is clearly unsuitable as a structural steel for building construction purposes due to its very high room temperature yield strength, 594 MPa. However, the P8124 experimental steel represents a change in direction for fire-resistant steels. It has low carbon content, is thermally stable and has a totally ferritic microstructure, so it does not have the overageing problems of ferrite/pearlite steels. The upper temperature limit for phase stability and good strength imposed by the ferrite to austenite phase transformation is very high, at around 920 °C. It is difficult to separate the effect of its large grain size from its high friction stress and the volume fraction of Laves phase particles. Transmission electron microscopy (TEM) has shown that they are present in this steel even after heat treatment at 750 °C. Therefore, it is thought that the Laves phase particles are responsible for the good high temperature strength of the P8124 steel, as well as the large grain size and the high friction stress of the elements in solid solution.

It has also been shown that the elongation of the P8123 and P8124 steels is not adequate for structural steels and that grain boundary precipitation is the cause of

the poor elongation. Therefore, this property needs to be improved in future steels. It is of scientific interest to design a type of steel based almost entirely on solid solution effects. Solid solution steel has never been used for high temperature use in the past to the author's knowledge.

The experimental steels almost certainly provide 30-min fire resistance for an unprotected I-beam, achieving the target fire-resistance set out before their design.

References

Sha W (2001) Mechanical properties of structural steels with fire resistance. In: Hanada S, Zhong Z, Nam SW, Wright RN (eds) The fourth Pacific Rim international conference on advanced materials and processing. The Japan Institute of Metals, Sendai, pp 2707–2710

Sha W, Kelly FS (2004) Atom probe field ion microscopy study of commercial and experimental structural steels with fire resistant microstructures. Mater Sci Technol 20:449–457. doi:10.1179/026708304225012305

Sha W, Kelly FS, Browne P, Blackmore SPO, Long AE (2002) Development of structural steels with fire resistant microstructures. Mater Sci Technol 18:319–325. doi:10.1179/026708301225000789